Apoptosis 2006; 11: 749–764

DOI: 10.1007/s10495-006-5697-7

Induction of three-dimensional assembly and increase in apoptosis of human endothelial cells by simulated microgravity: Impact of vascular endothelial growth factor

M. Infanger, P. Kossmehl, M. Shakibaei, S. Baatout, A. Witzing, J. Grosse, J. Bauer, A. Cogoli, S. Faramarzi, H. Derradji, M. Neefs, M. Paul and D. Grimm

Department of Trauma and Reconstructive Surgery, Charité-University Medical School, Benjamin Franklin Medical Center Center of Space Medicine Berlin, 12200 Berlin, Germany (M. Infanger); Institute of Clinical Pharmacology and Toxicology, Charité-University Medical School, Campus Benjamin Franklin, Center of Space Medicine, 14195 Berlin, Germany (P. Kossmehl, A. Witzing, J. Grosse, S. Faramarzi, M. Paul, D. Grimm); Institute of Anatomy, Charité-University Medical School, Campus Benjamin Franklin, 14195 Berlin and Institute of Anatomy, Ludwig-Maximilians-University, 80336 Munich, Germany (M. Shakibaei); Laboratory of Radiobiology, Belgian Nuclear Research Centre, SCK-CEN, 2400 Mol, Belgium (S. Baatout, H. Derradji, M. Neefs); Max-Planck Institute of Biochemistry, 82152 Martinsried, Germany (J. Bauer); Zero-g Lifetec GmbH, Technopark, ETH Zurich, 8005 Zurich, Switzerland (A. Cogoli)

Published online: 9 March 2006

Endothelial cells play a crucial role in the pathogenesis of many diseases and are highly sensitive to low gravity conditions. Using a three-dimensional random positioning machine (clinostat) we investigated effects of simulated weightlessness on the human EA.hy926 cell line (4, 12, 24, 48 and 72 h) and addressed the impact of exposure to VEGF (10 ng/ml). Simulated microgravity resulted in an increase in extracellular matrix proteins (ECMP) and altered cytoskeletal components such as microtubules (alpha-tubulin) and intermediate filaments (cytokeratin). Within the initial 4 h, both simulated microgravity and VEGF, alone, enhanced the expression of ECMP (collagen type I, fibronectin, osteopontin, laminin) and flk-1 protein. Synergistic effects between microgravity and VEGF were not seen. After 12 h, microgravity further enhanced all proteins mentioned above. Moreover, clinorotated endothelial cells showed morphological and biochemical signs of apoptosis after 4 h, which were further increased after 72 h. VEGF significantly attenuated apoptosis as demonstrated by DAPI staining, TUNEL flow cytometry and electron microscopy. Caspase-3, Bax, Fas, and 85-kDa apoptosis-related cleavage fragments were clearly reduced by VEGF. After 72 h, most surviving endothelial cells had assembled to three-dimensional tubular structures. Simulated weightlessness induced apoptosis and increased the amount of ECMP. VEGF develops a cell-protective influence on endothelial cells exposed to simulated microgravity.

Keywords: apoptosis; endothelial cells; extracellular matrix proteins; microgravity, VEGF; weightlessness.

Introduction

Over the past 40 years many space missions have shown that prolonged exposure of humans to space radiation and extended weightlessness may seriously affect their health.[1] Prolonged stays in orbit increase the risk of bone loss and fracture, and reduce muscle mass.[1,2] Postflight orthostatic intolerance, cardiac atrophy and cardiac susceptibility to ventricular arrhythmias can occur.[3,4] Already at the beginning of a flight, space motion sickness has been repeatedly experienced.[5] In addition, cardiovascular problems and orthostatic hypotension have been reported.[6,7] Moreover, circadian rhythm-related problems involving sleep and performance,[8] as well as immune-related health concerns involving infections and immunodeficiency[9,10] were observed during and after space flights.

The effects of weightlessness on different cell types are currently a topic of interest. Many of the above mentioned health problems are due to the effects of weightlessness on cellular features. Alterations of the cytoskeleton,[11–13] loss of activation of T-cells[14] and changes in gene expression patterns[15,16] were observed. Under conditions of simulated weightlessness, reproducibly, three-dimensional growth of normal cells[17–20] and tumor cells[11,17,21] is induced, microtubule and mitochondria organization is altered,[11,13] the production of extracellular matrix and cytoskeletal proteins is modified,[13,17] and apoptosis is induced in different types of cells.[11,13,17]

Endothelial cells are one type of cells which are affected by weightlessness.[22,23] They form the endothelium, which is located at the interface between the blood and the vessel wall. The endothelium of all blood vessels is highly specialized with endocrine, exocrine, cell adhesion, clotting and transport functions. It plays a critical role in the mechanics of blood flow, the regulation of coagulation, leukocyte adhesion, and vascular smooth muscle cell growth, and also serves as a barrier to the transvascular diffusion of liquids and solutes. It can adapt rapidly to changes in its environment.[24,25]

Correspondence to: D. Grimm, MD Institute of Clinical Pharmacology and Toxicology, Charit-University Medicine, Campus Benjamin Franklin, Garytraße 5, 14195 Berlin, Germany. Tel.:+49-30-8445-1707; Fax: +49-30-8445-1762; . e-mail: daniela.grimm@charite.de

The endothelial cells are in close contact and form a smooth layer that prevents blood cell interaction with the vessel wall. Ultrastructurally, each cell can be seen to be anchored to an underlying basal lamina. Individual cells are anchored together by adhesion junctions, including prominent tight junctions, which prevent diffusion between cells. Endothelial cells may respond to changes in local conditions such as blood pressure, oxygen tension and blood flow by secreting substances, which have powerful effects on the tone of vascular smooth muscle. Under certain circumstances, especially in response to adverse stimuli such as wounds, infections or tumor challenge, the endothelial cell may become activated and change its function. In tissue regeneration endothelial cells contribute to the formation of new vessels. This process called angiogenesis may be mediated by proliferation, migration, and remodeling of fully differentiated endothelial cells from preexisting vessels.[26–28]

We intend to investigate whether weightlessness affects endothelial cell morphology, and protein expression because the endothelial cells play a crucial role in the maintenance of the functional integrity of the vascular wall, and also orthostatic and cardiovascular deconditioning[3,4,6,7] has been described in astronauts. Changes in differentiation, mechanisms of apoptosis and extracellular matrix and cytoskeletal proteins will be addressed. Molecular biological methods along with morphological techniques will be applied. In addition, our objective was to investigate whether the vascular endothelial growth factor (VEGF) would be able to counterbalance the changes caused by alteration of the physical parameter of gravity. VEGF comprises a family of secreted polypeptides, which predominantly affect endothelial cells.[29,30] They are responsible for the formation of new blood vessels during embryogenesis and in many pathological conditions.[31] In addition, they show neurotrophic, lymphangiogenic and endothelium protective activity.[31–33] The cell-protective activity of VEGF is a main focus of this investigation. Our study will also help to understand the basic changes of endothelial cells in microgravity and their possible role in altering the physiology of the vascular tree.

Material and methods

Random positioning machine (RPM)

The RPM, or three-dimensional clinostat, developed by T. Hoson and collaborators[34] in Japan, was manufactured by Dutch Space, Leiden, NL. On the RPM, the samples are fixed as close as possible to the center of the inner rotating frame. This frame is rotating within another rotating frame. Both frames are driven by separate motors. The rotation of each frame is randomly and autonomously regulated by computer software. Gravimeters fixed to the frame permit recording the gravity vectors during rotation. The electronic box installed in the inner frame, powers the experiment. Cell culture containers can be fixed in the center of the RPM. The RPM can be operated either as a random walk 3d-clinostat (basic mode), as a 2d-clinostat or as a centrifuge. The RPM is located in a room, thermostated at $37\pm1^{\circ}C$.

Cell culture procedure

The EA.hy926 cells were grown in DMEM (Invitrogen, Eggenstein, Germany). The medium was supplemented with 10% fetal calf serum (FCS) (Invitrogen, Eggenstein, Germany), 100 units penicillin/ml and 100 μg streptomycin/ml. Subconfluent monolayers (5×10^6 cells/flask) were randomized to the following study groups: six static incubator controls, sixty ground controls (4, 12, 24, 48, and 72 h; $n = 12$ each group), and sixty samples for the clinorotation experiments (4, 12, 24, 48, and 72 h; $n = 12$ each group). Static ground controls and clinorotation samples were randomized to receive either vehicle (NaCl 0.9%) or VEGF (10 ng/ml; Chemicon, Hofheim, Germany). The substances were diluted in complete medium and added to a 25 cm^2 (50 ml) culture flask (Sarstedt,Nümbrecht,Germany).

Ground controls are cultures kept in the same room as the RPM. To start a clinorotation culture, the culture flasks were filled with complete medium with a syringe, taking care to avoid air bubbles. The filled culture flasks were fixed onto the clinostat. The system was placed in a room with a temperature of 37°C. Rotation was 60°/s. Rotation time was 4, 12, 24, 48 and 72 h. Complete medium was changed every day.

Determination of micromilieu

To measure pH, bicarbonate, natrium, potassium, $p0_2$ and $pC0_2$ content in EA.hy926 cell culture supernatants, a commercially available radiometer (EML 100, Radiometer Copenhagen, Denmark) was used.

Microscopy

Cells grown in plastic culture flasks (Sarstedt, Nümbrecht, Germany) and three-dimensional endothelial cell aggregates were examined by phase contrast microscopy (Olympus, Hamburg, Germany). After labeling with fluorescent dyes (propidium iodide, DAPI) single cells were investigated by fluorescence microscopy (Leitz, Wetzlar, Germany).[36,37]

Histological staining

Endothelial cells were stained with hematoxylin and eosin for histological analysis.[38]

Immunocytochemistry

For immunofluorescence staining, cells were seeded out into one of a 4-chamber supercell chamber slide (BD,

Heidelberg, Germany) and incubated for 2 h (adhesion time). Subsequently, the monolayers were washed twice in PBS, fixed with methanol and ethanol (1:2, room temperature, 30 min) or 4% paraformaldehyde (4°C). The cells were washed twice in PBS again and then incubated with the first antibody for 24 h at room temperature (RT). The morphology of the microtubule cytoskeleton (alpha-tubulin; 1:100; Sigma, Taufkirchen, Germany) and intermediate filaments (pan-cytokeratin, 1:50, Sigma, Taufkirchen, Germany) were evaluated by indirect immunofluorescence and analyzed with a Zeiss 510 META inverted confocal laser scanning microscope equipped with a Plan-Apochromat 63×1.4 objective. Excitation and emission wavelengths were: $\lambda_{exc} =$ 364 nm and $\lambda_{em} = \geq$475 nm for DAPI and $\lambda_{exc} =$ 488 nm and $\lambda_{em} = \geq$505 nm for FITC.

The antibodies used for the immunolocalization study were directed against collagen type I (1:100), fibronectin (1:50) (both Chemicon, Hofheim, Germany), laminin (1:20), chondroitin sulfate (1:200; Sigma, Deisenhofen, Germany), activated caspase-3 (1:10, Chemicon), VEGF-A (1:50; Chemicon), flk-1 (1:800; Chemicon), bax (10 μg/ml; Chemicon), bcl-2 (prediluted; Chemicon), Fas (1:20; Chemicon), PARP (1:50; BD, Heidelberg, Germany), osteopontin (1:100; Developmental Studies Hybridoma Bank, University of Iowa, Department of Biological Sciences, Iowa, USA) and NFκb (1:100; Biocarta, Hamburg, Germany). Antigen-antibody complexes were visualized with the indirect immunofluorescence technique.[11,17] They were then rinsed in PBS and incubated for 24 h with anti-mouse/rabbit FITC-conjugated immunoglobulin antibody (DAKO, Hamburg, Germany). After washing in PBS, the cells were incubated with Propidium iodide (Molecular Probes, Eugene, OR, USA) for 1 h at 37°C. Then, they were rinsed again in PBS, mounted with Vectarshield immunofluorescence mounting medium (Vector, Burlingame, CA, USA) and sealed with nail polish.

Evaluation of apoptosis: DAPI staining and TUNEL detection

The cells for DAPI staining, including incubator controls, were fixed with 4% formaldehyde and incubated in the DAPI medium containing 4′, 6-diamidino-2-phenylindole (Molecular Probes, Eugene, OR). Stained nuclei were investigated using fluorescence microscopy.[11,17]

The TUNEL test was performed by flow cytometry using the MEBSTAIN Apoptosis Kit Direct (Medical and Biological Laboratories, Immunosource, Belgium). The protocol is based on the TdT-mediated FITC-dUTP nick end-labeling (TUNEL) method which labels the 3-OH ends of DNA strand breaks generated by apoptosis. Briefly, EA.hy926 cells (1×10^6) were fixed by 4% paraformaldehyde at 4°C, followed by two washings with PBS containing 0.2% Bovine Serum Albumin (BSA). Cold 70% ethanol was added to the cell pellet. Cells were then incubated for 30 min at −20°C for permeabilization. After washing twice with PBS containing 0.2% BSA, terminal deoxynucleotidyl transferase (TdT) reaction reagent was added to the cell pellet and incubated for 1 h at 37°C. The cell pellet was washed twice with PBS containing BSA and resuspended in 700 μL of the buffer before the sample was analysed by flow cytometry. Forward scatter, side scatter and green fluorescence (FITC-dUTP + TDT) were measured using an EPICS XL flow cytometer (EPICS XL, Beckman-Coulter, Analis, Belgium) equipped with an argon ion laser with an excitation wavelength at 488 nm. A threshold on the forward scatter was used in order to not take into account the cell debris.

Before each experiment, the instrument was calibrated with fluorescent beads (Flow-Check, Beckman-Coulter). The beads were uniform, with coefficients of variation always $\leq$2% for size and fluorescence. Software discriminators were set on forward side scatter (FS) signals to eliminate electronic and small particle noise. A total of 10.000 cells was recorded for each sample and all experiments were conducted in triplicates. A calibration curve to transform the mean channels of green fluorescence (corresponding to the amount of dUTP incorporated into damaged DNA by the TdT enzyme) was performed using Spherotech beads (RCP-30-5A, Libertyville, Illinois, USA) and, therefore, all results obtained in mean channel were transformed into Molecules of Equivalent Fluorescein (MEFL). Data were stored as list-mode files and analysed off-line using the System II software (Beckman-Coulter). Cells incubated in the absence of TdT were used as negative controls and cells treated with DNase I (100 μg/mL) for 1 h at 37°C were used as positive controls for voltage and gain adjustments and assignment of histogram regions. Values of MEFL for the negative controls were substracted from the values of MEFL of the equivalent samples.

Image analysis

Image analysis, was applied to quantitatively assess altered cells and nuclei (DAPI and propidium iodide staining) by using a video camera combined with a separate video control system (Sony MC-3255, AVT- Horn GmbH) adapted to a Zeiss Axiophot microscope (Oberkochen, Germany). Image analysis was performed with the use of freely available software (Scion Image 1.62a, Scion Co) on a Power Macintosh 8200/120 computer. The magnification was 10-fold.

Transmission Electron Microscopy (TEM) and quantitative image analysis

Tissue samples were fixed in 1% glutaraldehyde plus 1% tannic acid in 0.1 M phosphate buffer (pH 7.4), and were post-fixed in 2% OsO_4 in phosphate buffer. After rinsing and dehydration in ethanol, the samples were embedded in Epon (Plano, Marburg, Germany), cut on a Reichert Ultracut

followed by contrasting with 2% uranyl acetate/lead citrate. The specimens were examined with a transmission electron microscope (TEM 10, Zeiss, Oberkochen, Germany). A detailed description of the technique used for the following experiments has already been published by Shakibaei *et al*.[39] Ultrathin sections of all samples of the cell cultures were prepared, stained with 1% toluidine blue in 1% sodium tetraborate solution and evaluated under high resolution light microscopy to demonstrate the tubular structures. For statistical analysis ultrathin sections of the samples of the cells were prepared and evaluated with an electron microscope (Zeiss EM 10). The number of cells was determined by scoring 100 cells from 15 different microscopic fields.

Western blot analysis

SDS-PAGE and immunoblotting were carried out following routine protocols.[11,17,40] Six replicates have been performed. Antibodies against the following antigens were used for this study: collagen type I (1:1000), fibronectin (1:1000; polyclonal, Chemicon, Hofheim, Germany), laminin, chondroitin sulfate (1:1000; Sigma, Taufkirchen, Germany), and PARP (1:1000; BD, Heidelberg, Germany), activated caspase-3, Fas, Bax and bcl-2, flk-1, and VEGF (all diluted 1:1000; Chemicon, Hofheim, Germany), osteopontin (1:1000; Developmental Studies Hybridoma Bank, University of Iowa, Department of Biological Sciences, Iowa, USA), beta-actin (1:500; Sigma, Taufkirchen, Germany) and NFκb (1:2000; Biocarta, Hamburg, Germany).

The samples were homogenized by shearing forces in lysis buffer (50 mM Tris-HCl, pH 7.2, 150 mM NaCl, 1% Triton X-100, 1 mM sodium orthovanadate, 50 mM sodium pyrophosphate, 100 mM sodium fluoride, 0.01% aprotinin, 4 μg/ml pepstatin A, 10 μg/ml leupeptin, 1 mM phenylmethylsulfonyl fluoride "PMSF") on ice for 30 min. For immunoblotting, equal amounts of total proteins were separated by electrophoresis using 10% sodium dodecyl sulfate-polyacrylamide gels under reducing conditions. Subsequently, the homogenates were transferred onto a nitrocellulose membrane (Schleicher & Schüll, Dassel, Germany) using a transblot electrophoresis apparatus (Mini Trans BlotTM, BioRad Laboratories, Richmond, USA) for 1 h at 120 V. Membranes were blocked with 5% (w/v) skimmed milk powder in PBS/0.1% Tween 20 overnight at 4°C and incubated with primary antibodies diluted in blocking buffer for 1 h at RT. After five washes in blocking buffer, membranes were incubated with alkaline phosphatase-conjugated secondary antibody diluted in blocking buffer for 30 min at RT. Membranes were finally washed 5 times in blocking buffer, twice in 0.1 M Tris, pH 9.5, containing 0.05 M $MgCl_2$ and 0.1 M NaCl; specific binding was detected using nitro blue tetrazolium and 5-bromo-4-chloro-3-indoyl-phosphate (p-toluidine salt; Pierce, Rockford, IL, USA) as substrates and quantitated by densitometry (Molecular Dynamics Personal Densitometer No. 50301, Krefeld, Germany). Protein determination was done with the bicinchonic acid system (BCA; Pierce, Rockford, IL, USA) using BCA as a standard.

Statistical evaluation

Statistical analysis was performed using SPSS 11.5. All data are expressed as means $\pm$ standard deviation (SD). We tested all parameters for deviations from Gaussian distribution by Kolmogorov-Smirnov test and compared the cases by the use of independent – samples *t*-test or Mann-Whitney test (dependent on the results from the normality test). Differences were considered significant at the level of $P \leq 0.05$.

Results

Micromilieu

Clinorotation of EA.hy926 cells had no influence on the cellular micromilieu relative to pH (P = ns; 4, 12, 24, 48, and 72 h, vs. incubator and ground controls), natrium and potassium (P = ns; 4, 12, 24, 48, and 72 h vs. incubator and ground controls), bicarbonate (P = ns; 4, 12, 24, 48, and 72 h vs. incubator and ground controls) and $pC0_2/p0_2$ (P = ns; 4, 12, 24, 48, and 72 h vs. incubator and ground controls) content of all EAhy 926 cell cultures.

Morphology of endothelial cells cultured under simulated microgravity

After 12 h of clinorotation of a subconfluent monolayer, the formation of cell aggregates was visible in all culture flasks fixed on the three-dimensional RPM (Figure 1A). After 24 h, most endothelial cells had detached from the bottom of the culture flasks and several cell aggregates had formed and were floating in the medium under low-gravity conditions. After 48 h, nearly all cells were growing in the form of three-dimensional cell aggregates of different sizes. The aggregates formed by endothelial cells were of tubular shape. Maximum size of these structures was 1.8 $\pm$ 0.01 mm in length and 0.3 $\pm$ 0.01 mm in diameter. Three days of culture under simulated 0 g conditions revealed that no necrotic centers or areas were detectable as demonstrated by propidium iodide staining (Figure 1B and C). Microscopy of ultrathin slices documented the presence of organized cells around a lumen. The lumen is shown in Figure 1D and E.

Clinorotation changes extracellular matrix proteins

The clinorotated cells were harvested after 4 and 12 h, and the influence of simulated microgravity or VEGF, either alone or combined, was investigated for the expression of

Figure 1. (A) Phase contrast microscopy, multicellular tubular structure under conditions of simulated microgravity (24 h). This tube-like structure has a length of 1.8 mm. Propidium iodide staining: Longitudinal multicellular aggregate formed within 24 h of clinorotation and VEGF (B) and C: vehicle. D, E Semithin section of a tubular structure with a length of 1.8 mm, collected after 72 h culture under simulated microgravity. A lumen is visible. The picture shows that an artificial endothelium layer is formed along the extracellular matrix (arrows).

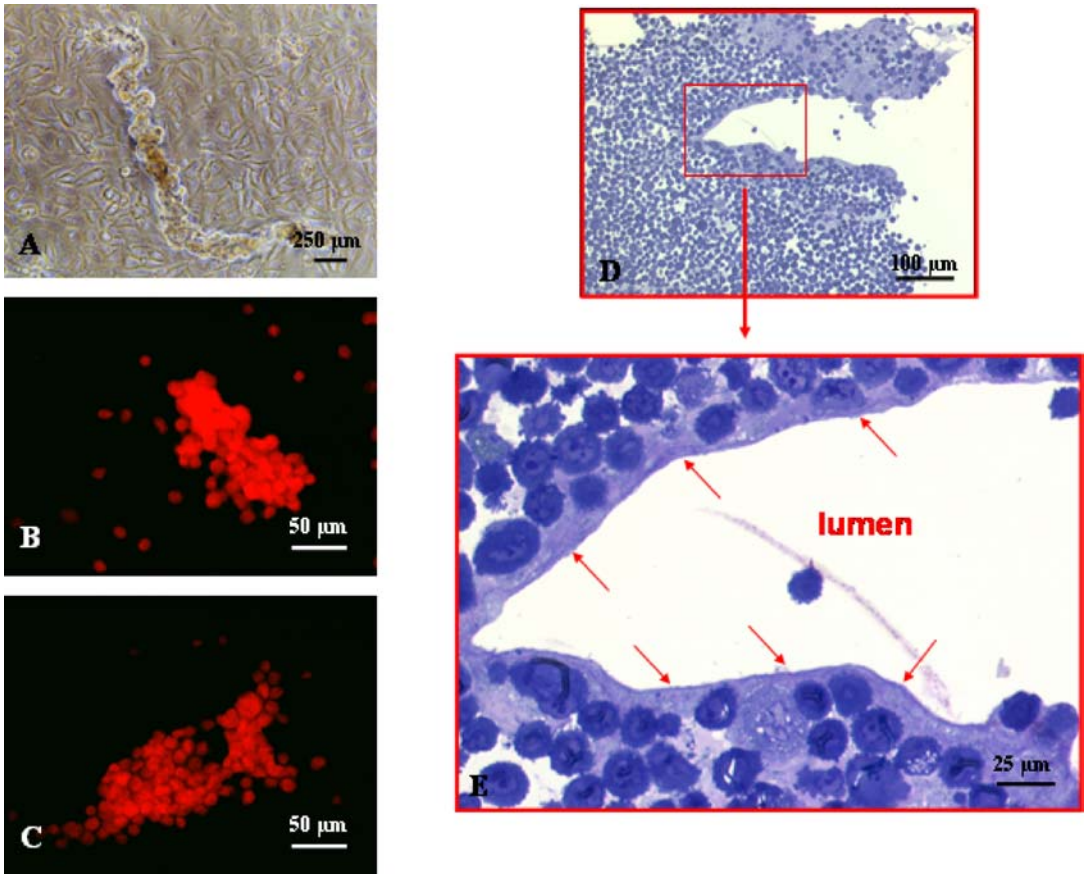

extracellular matrix components. Microgravity or VEGF application increased the expression of fibronectin, chondroitin sulfate, collagen type I, and laminin within 4 h to similar extents (Figure 2A–E), while OPN production was mainly increased by microgravity and not by VEGF (Figure 2D). Simulated microgravity and VEGF had no synergistic effects on the cellular synthesis of fibronectin, and chondroitin sulfate. The quantity of laminin under the simultaneous influence of microgravity and VEGF was slightly reduced compared to exposure to microgravity alone (Figure 2C). Immunolocalization of these extracellular matrix proteins revealed a cytoplasmic fluorescein immunostaining.

Furthermore, the endothelial cells, which had been exposed to simulated microgravity or to VEGF for 12 h, showed an increase in fibronectin, collagen type I, and laminin. But at this time point, the increase in all these components was more pronounced following exposure to simulated microgravity compared to VEGF. Osteopontin and chondroitin sulfate responded only to clinorotation but not to VEGF. Surprisingly, when VEGF was present in medium of clinorotated cultures for 12 h, the effect of microgravity on the expression of fibronectin, chondroitin sulfate, osteopontin, and laminin was reduced. These results suggest that VEGF may counterbalance the effects of simulated microgravity on those extracellular matrix components (Figure 2A–E) during the first 12 h of growth under conditions of simulated microgravity.

Impact of simulated microgravity on VEGF and flk-1 protein

VEGF is increased after 4 h of clinorotation and further elevated after 12 h. VEGF slightly reduced the protein in clinorotated cells after 4 and 12 h (Figure 3A). VEGF was localized in the cytoplasm of EA.hy926 cells.

Clinorotation early induced flk-1 protein (within 4 h). This increase was further elevated after 12 h of culturing the cells under simulated microgravity. VEGF treatment also increased flk-1 protein but clinorotation exhibited no further effect within 4 h. VEGF application for 12 h reduced the amount of flk-1 protein (Figure 3B). Flk-1 immunofluorescence staining of EA.hy926 cells revealed membrane staining.

Figure 2. Western blot analyses of extracellular matrix proteins: (A) Collagen type 1 protein is elevated by microgravity. VEGF application had no effect on collagen type I after 12 h. VEGF enhanced collagen type I in ground controls. Immunolocalization of collagen type I: Immunofluorescence staining of methanol-fixed EA.hy926 cells showing cytoplasmic immunostaining and nuclear propidium iodide counterstain. (B) Simulated microgravity increased fibronectin protein. VEGF treatment increased fibronectin in static ground controls and attenuated the amount of fibronectin protein in clinorotated cells after 12 h. Immunolocalization of fibronectin: Immunofluorescence staining of methanol-fixed EA.hy926 cells showing cytoplasmic immunostaining and nuclear propidium iodide counterstain. (C) Laminin protein is clearly increased after 4 h and 12 h of microgravity. VEGF decreased the amount of laminin protein in clinorotated cells and induced it in static ground control cells. Immunolocalization of laminin: Immunofluorescence staining of methanol-fixed EA.hy926 cells showing cytoplasmic and membrane immunostaining and nuclear propidium iodide counterstain. (D) Osteopontin is increased by clinorotation after 4 and 12 h. VEGF significantly decreased osteopontin in clinorotated endothelial cells after 12 h of microgravity. Immunolocalization of osteopontin: Immunofluorescence staining of methanol-fixed EA.hy926 cells showing cytoplasmic immunostaining and nuclear propidium iodide counterstain. (E) Chondroitin sulfate protein is elevated by microgravity (4 h). VEGF induced chondroitin sulfate to similar extents in both clinorotated samples and static controls. After 12 h, chondroitin sulfate was decreased compared with vehicle-treated clinorotated group but unchanged compared to the corresponding 1g group. Immunolocalization of chondroitin sulfate: Immunofluorescence staining of methanol-fixed EA.hy926 cells showing cytoplasmic immunostaining and nuclear propidium iodide counterstain.

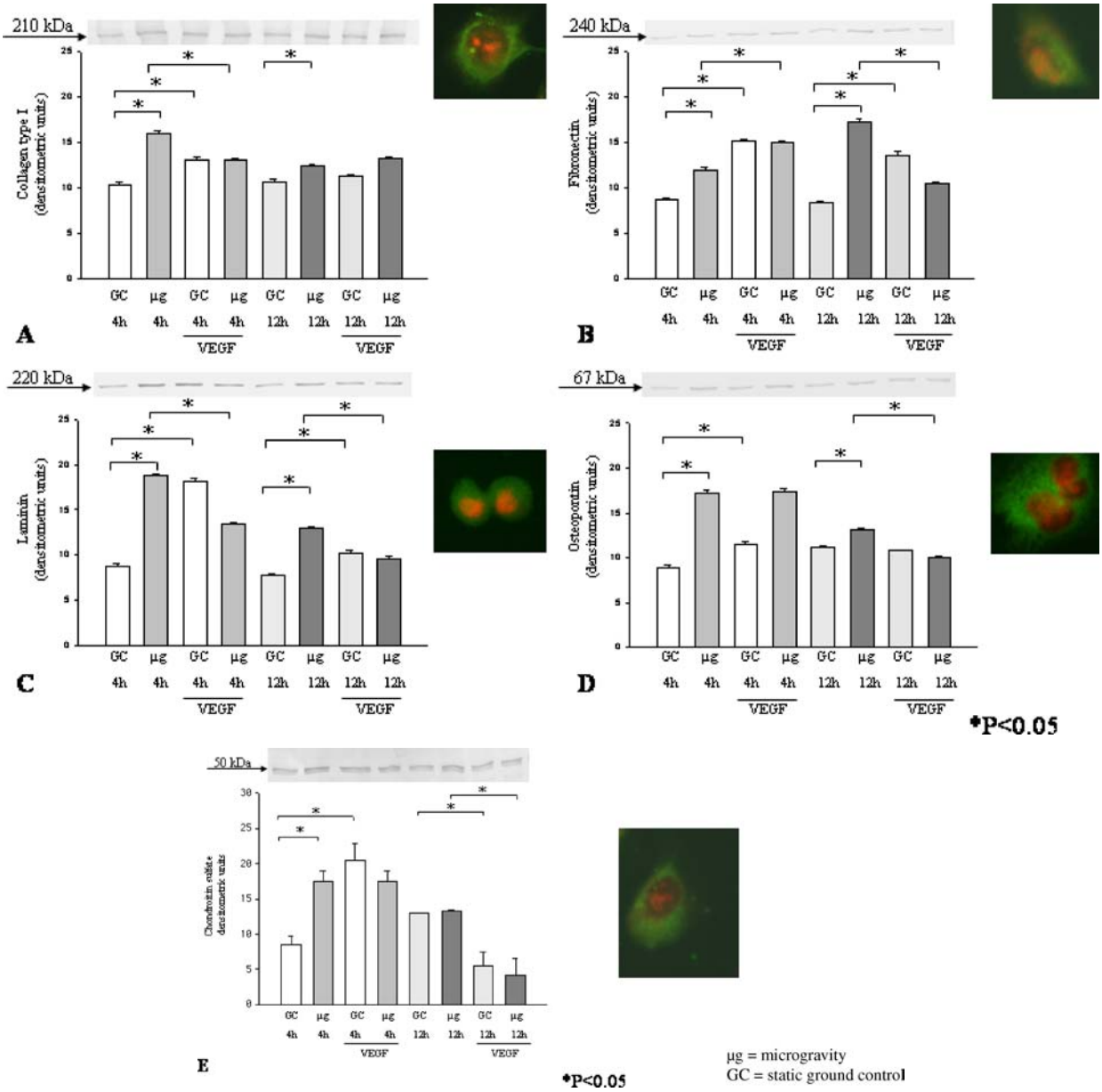

Figure 3. (A) VEGF is increased in vehicle treated groups by clinorotation compared with static ground controls ($P < 0.05$). Immunolocalization of VEGF: Immunofluorescence staining of methanol-fixed EA.hy926 cells showing cytoplasmic immunostaining and nuclear propidium iodide counterstain. (B) Flk-1 is enhanced by clinorotation. VEGF enhanced flk-1 in static ground controls. VEGF application reduced the amount of flk-1 protein after 12 h of clinorotation, no effect was seen after 4 h. Immunolocalization of flk-1: Immunofluorescence staining of methanol-fixed EA.hy926 cells showing membrane localization and nuclear propidium iodide counterstain.

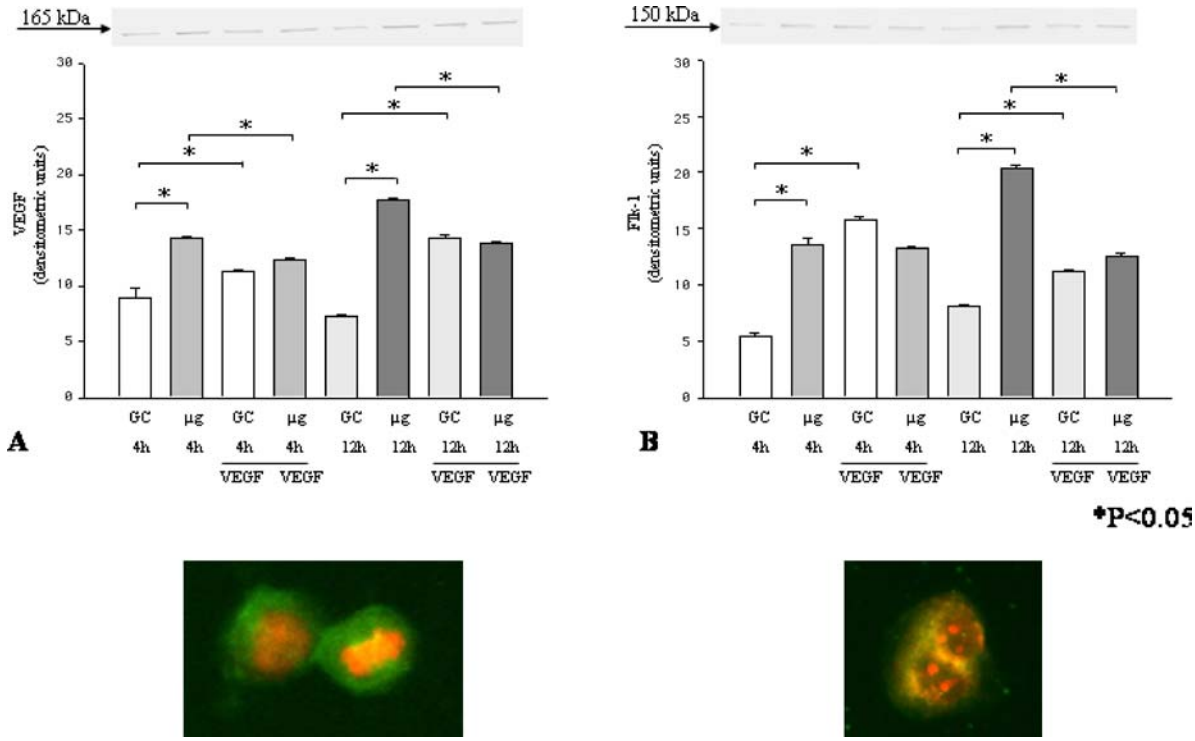

Apoptosis in endothelial cells cultured under simulated microgravity

Electron microscopy revealed chromatin condensation in nuclei of endothelial cells cultured for 4 h on the RPM. Apoptosis was found only in the absence of VEGF, but not in its presence. In the absence of VEGF, cell destruction continued during clinorotation up to 72 h. Moreover, apoptotic bodies were visible. When VEGF was present, however, nuclei in an increased number of endothelial cells resembled the controls, indicating a cell-protective ability of VEGF under conditions of weightlessness (Figure 4). Statistical evaluation proved the cell-protective effects of VEGF (Figure 4I).

Propidium iodide staining revealed characteristics of apoptosis such as chromatin condensation and the occurrence of apoptotic bodies in endothelial cells cultured under 0g. VEGF treatment reduced the amount of apoptotic cells compared to static controls (Figure 5).

DAPI staining of 72 h old clinorotated samples revealed a clearly elevated rate of apoptotic endothelial cells. VEGF treated cells significantly attenuated the amount of apoptotic cells (Figure 6). Incubator and static ground controls exerted no signs of apoptosis. All cells were viable.

Using the TUNEL assay, the DNA fragment multimers of approximately 180–200 bp in length were fluorescently labeled and were quantitated by flow cytometry. Figure 7 shows the results of the TUNEL procedure performed using the MEBSTAIN Apoptosis Kit Direct. EA.hy926 cells were cultivated for either 24 or 48 h. Figure 7 shows that clinostat conditions (24 and 48 h) induce a substantial increase in TUNEL Molecules of Equivalent Fluorescein (MEFL) in comparison with ground controls. The addition of VEGF to clinostat-cultivated cells induced a decrease in TUNEL MEFL showing a cell-protective effect of VEGF against clinostat-induced apoptosis. This data support the findings observed after DNA staining and electron microscopy.

Mechanisms of apoptosis in endothelial cells cultured under simulated microgravity

The cell-protective effect of VEGF under simulated microgravity was also demonstrated after 24 h. Activated caspase-3 was clearly enhanced in clinorotated samples after 24 and 72 h. VEGF attenuated this increase in clinorotated cultures. In static ground controls no activated caspase-3 was detectable (Figure 8A). Cytoplasmic staining of activated caspase-3 was observed in clinorotated samples.

Fas protein was increased in clinorotated samples after 24 h. VEGF application induced Fas in both, static ground controls and clinorotated samples. After 72 h culture in weightlessness, Fas is clearly elevated in clinorotated samples

Figure 4. Electron microscopy of human endothelial cells (EA.hy926 cell line): (A) Normal static ground control cells exhibited the characteristics of the cell line. (B) VEGF-treated cells showing signs of activation such as prominent nucleoli (arrows). (C) 4 h of culturing under conditions of zero-g: signs of apoptosis are visible. (D) 4 h of microgravity and VEGF: All cells are viable. VEGF has a clear cell-protective ability. (E) 72 h: Confluent layer of static ground control cells. (F) 72 h: VEGF treated sample of static ground control cells. An increase in extracellular matrix material is seen (M). A thickened basement membrane of the cells and an increase in extracellular matrix material is visible. (G) 72 h of culturing under conditions of microgravity. Apoptotic cell death is detectable including apoptotic bodies (arrows). (H) 72 h of microgravity and VEGF. The majority of endothelial cells were protected against apoptosis and viable. (I) Statistical evaluation of electron microscopic data: The number of cells was counted by scoring 100 cells from 15 different fields. The diagram shows the number of pathologically altered cells (mean values and standard deviations) of the results from three different samples.

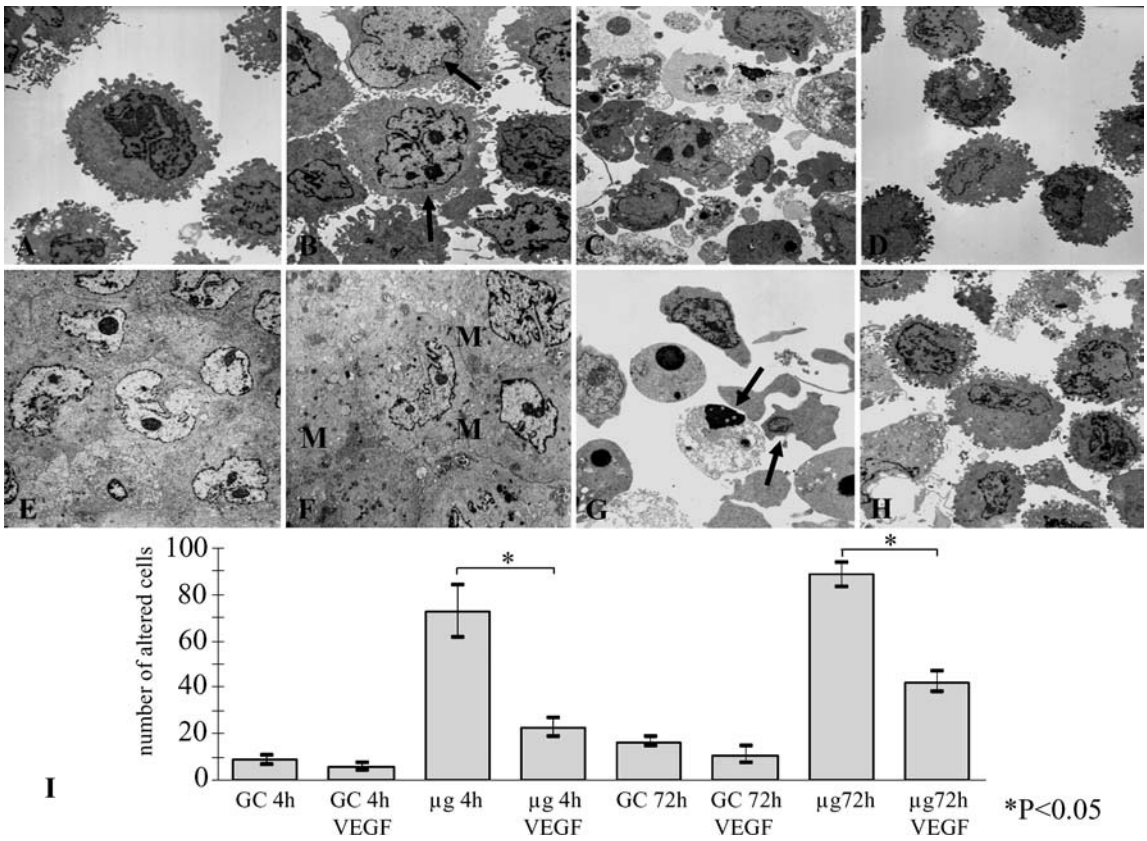

and normalized in the VEGF treated samples (Figure 8B). Fas immunofluorescence staining of EA.hy926 cells showed a membrane localization.

Bax was slightly increased after 24 h on the RPM. VEGF induced Bax in ground controls but reduced Bax protein in clinorotated cells within 24 h. After 72 h of culture in microgravity, Bax is clearly increased compared to static ground controls. VEGF attenuated the amount of Bax proteins to a normal level (Figure 8C). Bax was localized in the cytoplasm of EA.hy926 cells.

Bcl-2 protein was elevated by clinorotation. VEGF treatment clearly induced the amount of Bcl-2 protein in all clinorotated samples within 24 and 72 h (Figure 8D). Bcl-2 was localized in the cytoplasm of EA.hy926 cells.

These results indicate that simulated microgravity induced apoptosis via extrinsic and intrinsic pathways. It was initiated by external signals using the death receptor CD95, but also caspase-3 activation, changes in Bax and Bcl-2 were detectable.

In addition, NFκB is elevated early by clinorotation and further enhanced by VEGF combined with clinorotation compared to the corresponding static ground control cells. After 72 h of culture under simulated microgravity, NFκB is highly elevated by microgravity alone, but reduced by VEGF application (Figure 9). NFκB was detected in the cytoplasm of the EA.hy926 cells.

PARP and its 85-kDa cleavage fragment were increased by clinorotation after 24 and 72 h. VEGF reduced PARP after 24 and 72 h (Figure 10). PARP immunofluorescence revealed nuclear staining.

Investigation of the cytoskeleton of EA.hy926 cells

In the static ground control cells, cytokeratin networks displayed characteristic patterns depending on their intracellular localization (Figure 11A). After 24 h of clinorotation the intermediate filament network for cytokeratin had

Figure 5. Propidium iodide staining: (A) Static ground control cells with normal nuclei. (B) 24 h of clinorotation: Apoptotic cells are detectable. (C) 72 h of clinorotation: Apoptotic bodies (arrows) are visible. (D) VEGF treated clinorotated cells exhibited normal propidium iodide-stained nuclei. (E) Statistical analysis of propidium iodide staining.

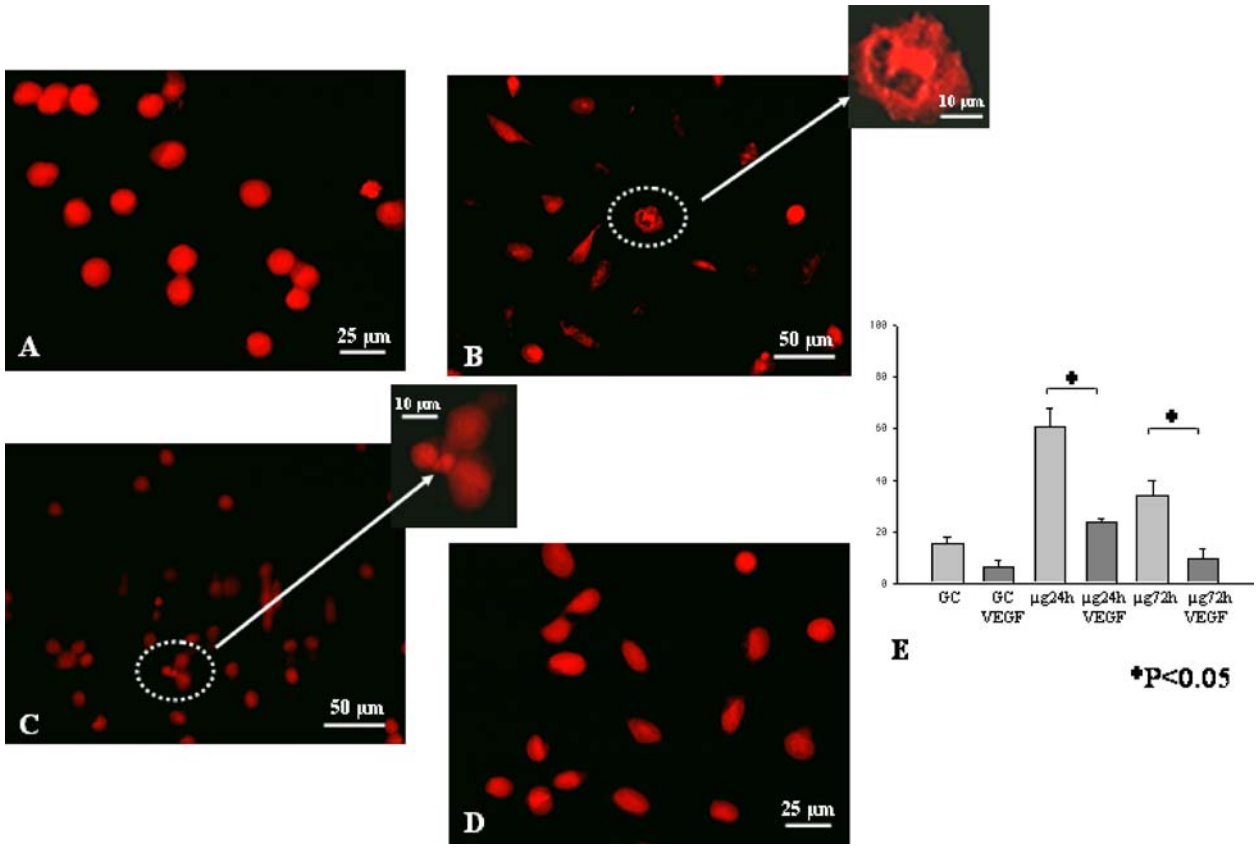

considerably increased (Figure 11B). cytokeratin was gathered in a dense center near the nucleus.

Microtubules (alpha-tubulin) radiated to the cellular membrane in static controls at 1g (Figure 11C). EA.hy926 cells exerted an increase in alpha-tubulin and many of the microtubules are coiled in close association with the nucleus when they grew under simulated microgravity for 24 h (Figure 11D).

Discussion

Amongst the observations demonstrated in this manuscript, the most significant and novel findings in endothelial cells cultured on a random positioning machine which simulates weightlessness were: first, the formation of three-dimensional tubular structures, second, the increase in extracellular matrix proteins, and third, the initiation of programmed cell death. Both of the latter effects were counterbalanced by VEGF application. In addition, clinorotated endothelial cells also produced more than normal amounts of VEGF and flk-1 by themselves. Moreover, simulated microgravity induced alterations of the cytoskeleton of human endothelial cells.

The random positioning machine (RPM) is a method for the simulation of weightlessness on earth

Clinostat and bioreactor systems have proved to be advantageous in a variety of experiments that are limited to the biological effects of real weightlessness in space and exclude effects of cosmic radiation. Applications include tissue engineering,[20] maintenance of normal prostate tissue[41] as well as studies on normal[42–44] and cancer cells.[45] Our group used the RPM to produce multicellular tumor spheroids of thyroid carcinoma cells.[11,17] Similar results can be obtained using a HARV (high aspect ratio vessel) NASA rotary cell culture system and various human tumor cell lines and fibroblasts in simulated microgravity. [45]

We investigated human endothelial cells on a three-dimensional RPM to characterize separate and common effects of simulated weightlessness and VEGF on this cell type. In contrast to other instrumentation available for simulated microgravity experiments such as the fast rotating clinostat[46] or the rotating wall vessel,[47] the RPM has two independent frames.[11,13,34] Its major advantage is a software that drives the motors of each frame to random and autonomous but simultaneously smooth and continuous,

Figure 6. DAPI staining of (A) Vehicle-treated clinorotated endothelial cells cultured under simulated microgravity for 72 h: Nuclei with chromatin condensation are seen. (B) VEGF-treated sample: There is a clear reduction of cells exhibiting chromatin condensation after 72 h. (C) Statistical evaluation of DAPI staining.

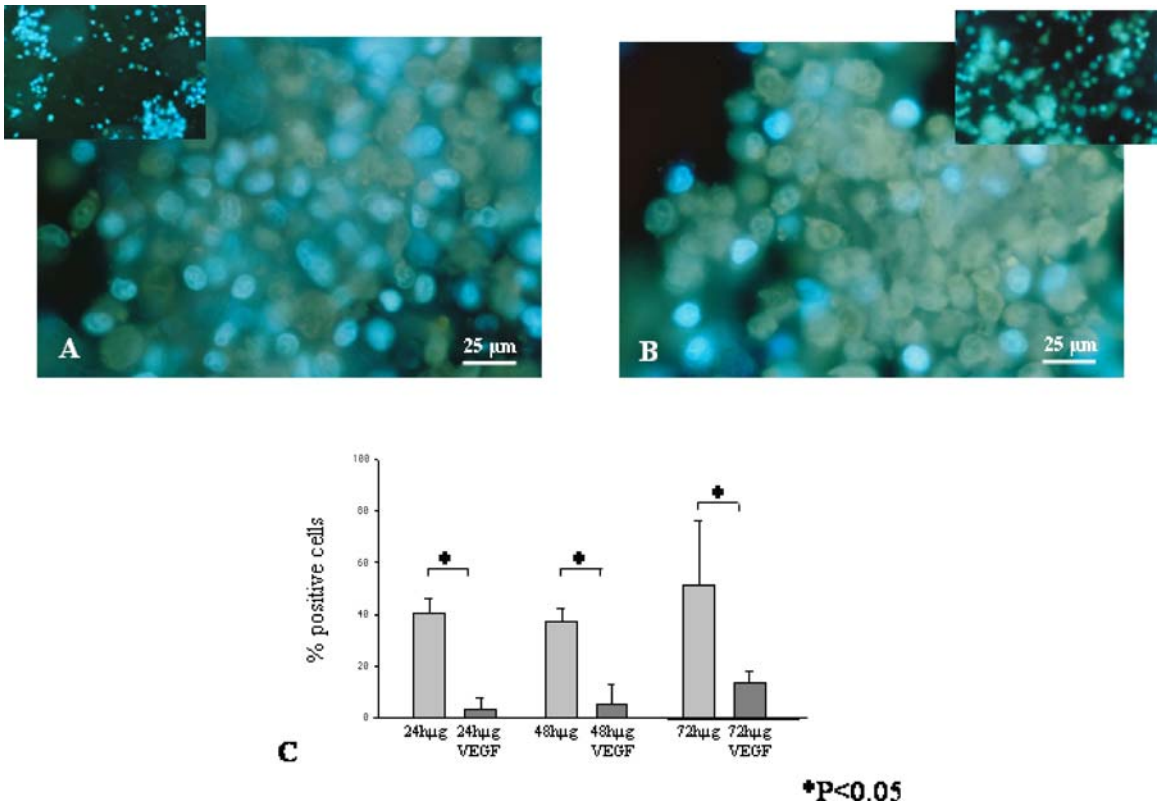

i.e. joltless, movement. So the locations and positions of cells in regard to gravity force vectors are changed quickly and smoothly. This prevents gravity forces from pulling the cells into one direction. The clinostat used is a reliable device to create vectorless conditions. In an earlier study the data obtained with human lymphocytes in the RPM were qualitatively and quantitatively nearly identical to those obtained in space. In fact the depression of the mitotic index after exposure to the mitogen concanavalin A was more that 80% in the RPM as well as in space.[48] Therefore, clinorotation is an important terrestrial model system for studying the effects of reduced gravity on cells in order to develop experimental systems and hypotheses concerning gravitational cell biology. It may help to find the roots of the negative physiological changes which humans and animals face during a longer stay in orbit.[1] The three-dimensional clinostat could also provide a convenient experimental system that allows the culture of many endothelial cells grown in the form of tubes. It may additionally become an important tool to trigger apoptosis under controlled physical conditions.

Formation of three-dimensional cell aggregates

The formation of tubular three-dimensional cell aggregates of the endothelial cells cultured under conditions of simulated microgravity was a surprise. It was known that EA.hy926 cells, like several types of endothelium related stem cells, form complex networks of cord- or tube-like structures when plated on an extracellular matrix material and cultured under appropriate conditions.[49–53] Here we demonstrate that EA.hy926 cells assemble to tube-like structures when they had detached from the bottom of a culture flask between the 12th and 48th hour under

Figure 7. Comparison of the TUNEL assay of EA.hy926 cell line in various culture conditions from top to bottom: ground control (GC) 24 h, clinostat (μg) 24 h, ground control + VEGF 24 h, clinostat + VEGF 24 h, ground control 48 h, clinostat 48 h, clinostat + VEGF 48 h. Means of 6 replicates ± standard errors of the mean (SEM) are shown. Statistical measurements are given.

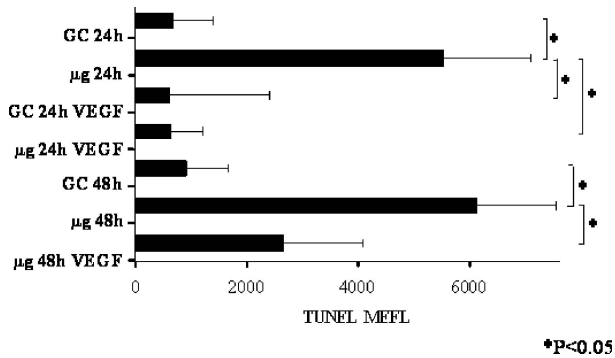

Figure 8. (A) Activated caspase-3 is elevated in all clinorotated samples. VEGF attenuated the amount of activated caspase-3 protein. Immunolocalization of caspase-3: Immunofluorescence staining of EA.hy926 cells showing cytoplasmic immunostaining and nuclear propidium iodide counterstain. (B) Fas protein is increased by clinorotation and elevated by VEGF after 24 h. After 72 h VEGF attenuated Fas protein in clinorotated samples. Immunofluorescence staining of methanol-fixed EA.hy926 cells showing membrane localization of Fas and nuclear propidium iodide counterstain. (C) Bax protein is increased by clinorotation and attenuated by VEGF after 72 h. Immunolocalization of Bax: Immunofluorescence staining of methanol-fixed EA.hy926 cells showing cytoplasmic immunostaining and nuclear propidium iodide counterstain. (D) Bcl-2 protein is clearly elevated by weightlessness, but also VEGF increased bcl-2 protein in static ground controls. During clinorotation bcl-2 remained elevated during 72 h. Immunolocalization of Bcl-2: Immunofluorescence staining of methanol-fixed EA.hy926 cells showing cytoplasmic immunostaining and nuclear propidium iodide counterstain.

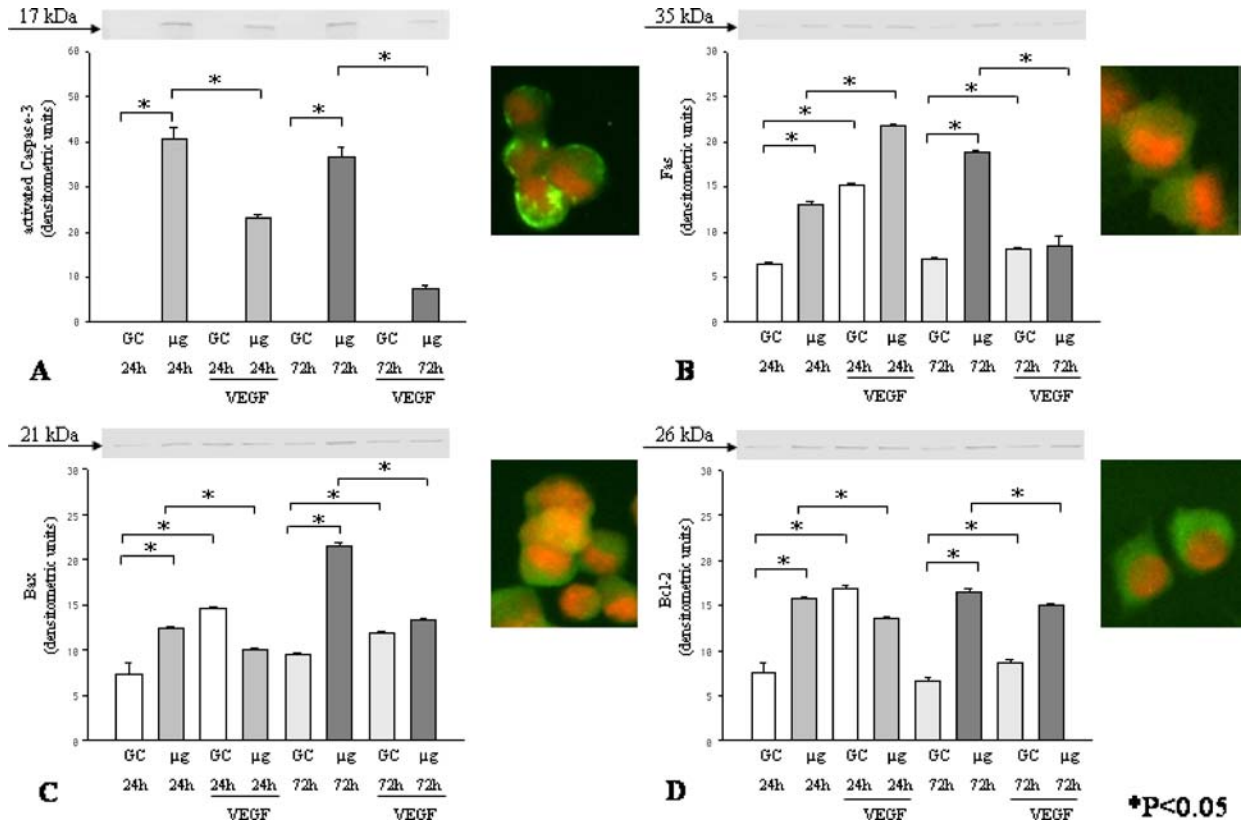

Figure 9. NFκB protein is induced by microgravity and early increased by VEGF. After 72 h VEGF reduced the amount of NFκB protein, whereas microgravity alone increased it. Immunolocalization of NFκB p65: Immunofluorescence staining of methanol-fixed EA.hy926 cells showing cytoplasmic localization. Nuclei are counterstained with propidium iodide.

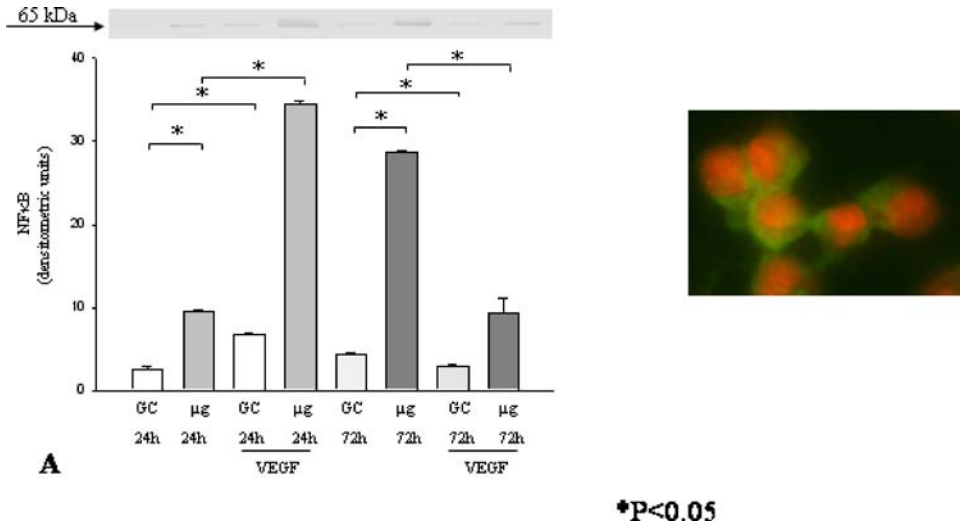

Figure 10. PARP 116 kDa (A) as well as PARP 85 kDa (B) are elevated by microgravity. VEGF application reduced the amount of PARP and its 85 kDa cleavage fragment after 24 h and 72 h. Immunolocalization of PARP: Immunofluorescence staining of methanol-fixed EA.hy926 cells showing nuclear localization. Nuclei are counterstained with propidium iodide. (C, D): Beta-actin as control protein (P = ns).

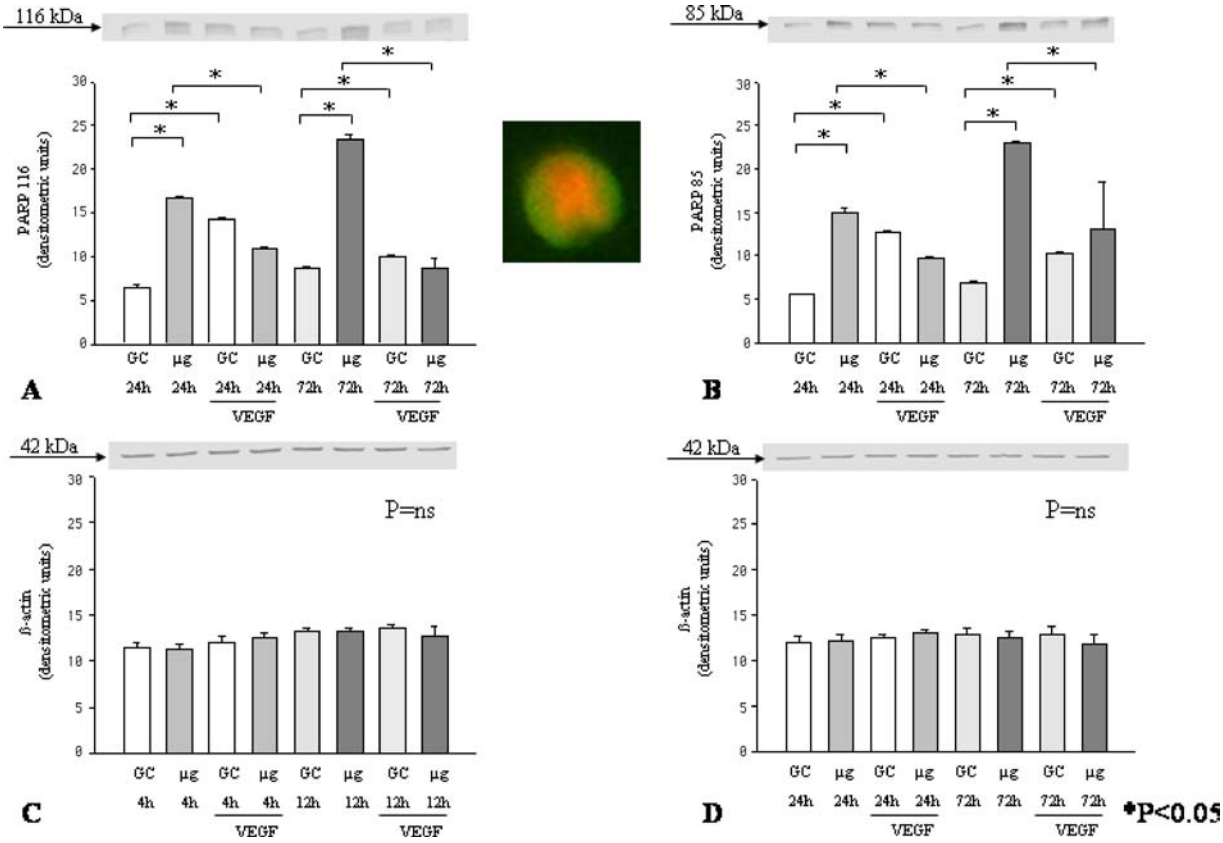

simulated microgravity. It is noteworthy that they do not form spheroids like the thyroid cells in other clinorotation experiments.[11,17] Thus, the kind of cell aggregates formed under microgravity seems to depend on the type of cells. This supports the idea that under microgravity, where cells keep floating without stirring- and gravity-related push or shear forces, cell-cell interactions are induced by forces exclusively due to biochemical components actually expressed on surfaces of cells. It also confirms an earlier observation that non-stem cells are able to create three-dimensional tube-like assemblies by culturing cells in microgravity[21] and points to the possibility that adult endothelial cells might be used for tube formation too. This could be an alternative model in studying the development of new blood vessels or in engineering tubes for surgical purposes. It has the advantage that the system consists only of endothelial cells and VEGF, while complex gels containing stimuli such as fibrinogen or platelet particles are not required.[50,51]

Effects of VEGF on extracellular matrix proteins

Endothelial cells increased their concentrations of extracellular matrix components compared to the corresponding static ground control cells. This phenomenon has already been observed on thyroid cancer cells and chrondrocytes exposed to simulated microgravity[11,17,54] as well as on bone cells flown through the space.[55] In many cases increased production of extracellular matrix is paralleled by enhanced production of cytoskeletal proteins.[11,17] Whether or not these observed alterations are due to a common pathway of regulation has to be determined.

VEGF and simulated microgravity alone enhanced the expression of fibronectin, chondroitin sulfate, collagen type I, osteopontin, and laminin similarly, but did not show synergistic effects when acting together within the early phase of 4 h of clinorotation. During a second phase, the VEGF influence ceased, while microgravity kept on increasing fibronectin, collagen type I, and laminin. When acting together in this phase, VEGF suppressed or reduced the microgravity dependent amount of fibronectin, chondroitin sulfate, osteopontin, and laminin.

This finding suggests that VEGF prevents an overproduction of ECMP, although extracellular matrix is required for tube formation.[56]

However, it is known that some ECM components such as Fibulin-5 and VEGF antagonize each other.[57] In addition, VEGF provides survival signals independent of its ability to promote matrix reattachment[58] and accelerates the rate of assembly and disassembly of focal adhesion complex.[59] Thus,

Figure 11. Immunofluorescence of anti-cytokeratin: (A) Normal distribution of cytokeratin filaments in EA.hy926 static control cells. (B) 24 h of clinorotation: The filaments became thicker and all EAhy926 cells were cytokeratin-positive. (C) alpha-tubulin: Static control (1g) cells. (D) Simulated microgravity (24 h): Microtubules became thicker and tubulin was gathered around the nucleus (Arrow).

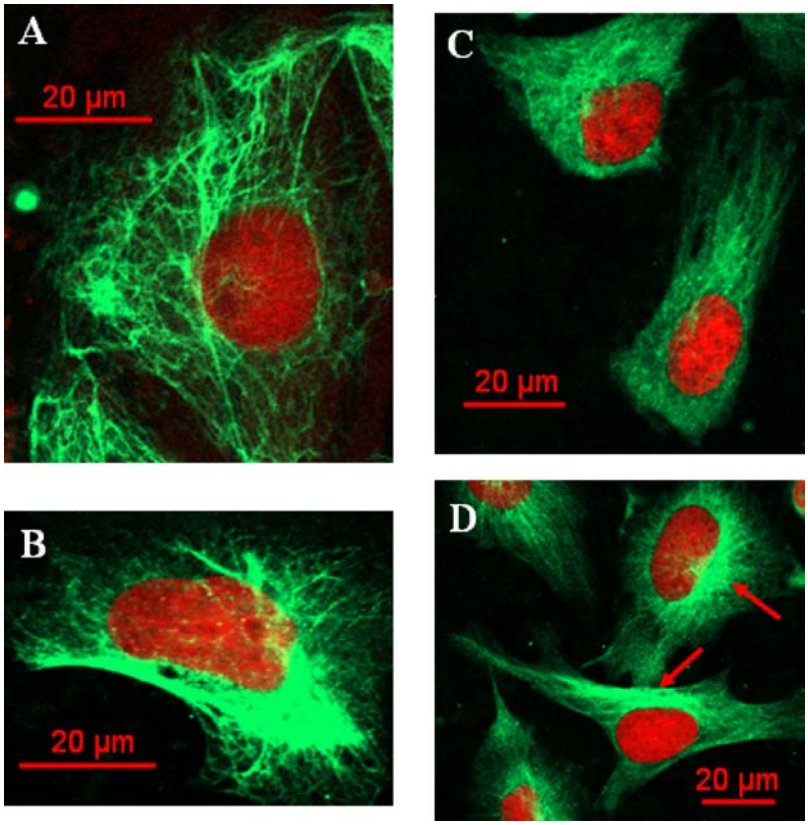

in the presence of VEGF the cells may stop overproduction of ECM components because they are not forced anymore.

Impact of VEGF on clinorotation induced programmed cell death

Moreover, we measured an increase in caspase-3 activation and detected characteristic morphological signs of programmed cell death, such as an elevated cleavage of 116-kDa PARP to the 85-kDa apoptosis-related cleavage fragment, and dye permeability as well as morphological changes. The observed responses of clinorotated cells are related to gravitational unloading because ground controls were negative for morphological signs of apoptosis as well as activated caspase-3 and bax proteins, but strongly positive for bcl-2. Bcl-2 as a pro-survival member of the Bcl-2 family can act by preventing the release of apoptotic molecules from organelles such as mitochondria.[60] These data are in agreement with our earlier results,[11,17] and with observations made on other cells exposed to real or simulated microgravity.[61,62] They confirm that programmed cell death was induced in many types of cells when grown under simulated microgravity.

Here we could show that VEGF has a cell-protective effect on endothelial cells cultured under simulated microgravity. When added to cultures before the start of clinorotation, VEGF reduced enhancement of extracellular matrix synthesis as well as initiation of apoptosis. Electron microscopy and quantitative image analysis revealed that VEGF significantly reduced programmed cell death induced by clinorotation up to 72 h. A significantly lower amount of cells showed characteristic signs of apoptosis such as apoptotic bodies, membrane blebbing and chromatin condensation in the presence of VEGF. These results are in accordance with earlier studies, which clearly showed that VEGF inhibits apoptosis of endothelial cells, induced by anchorage disruption or tumor necrosis factor alpha.[63,64]

Here we could show that the anti-apoptotic effects became dominant already after 4 h. During initial 24 h, microgravity upregulated the amount of Fas, NFkB, PARP-116 and PARP-85, Bax and bcl-2 as well as activated caspase-3. When acting together in this phase, the effects of microgravity on the expression of PARP-116 and PARP-85, Bax and bcl-2 were attenuated by VEGF, while Fas and NFkB were enhanced synergistically. After 72 h of clinorotation, microgravity had further enhanced the cellular concentrations of Fas, Bax, Bcl-2, NFkB, PARP-116 and the PARP-85 cleavage fragment, compared to static controls. If VEGF was present in clinorotated cultures, it clearly counterbalanced the microgravity effects on Fas, PARP-116, PARP-85, NFκB, and Bax. Interestingly, activation of caspase-3

was reduced by VEGF by one third after 24 h and by two thirds after 72 h, but never augmented. These data indicate that VEGF acts via intrinsic pathways by reducing Bax. Moreover, activated caspase-3 was reduced by VEGF. In parallel, also the extrinsic pathway is addressed by VEGF. A recent paper also reported about an increased gene expression of apoptotic signals in porcine endothelial cells cultured under zero-g.[65]

The observed responses of clinorotated cells are related to the microgravity environment because ground controls and incubator controls were negative for morphological signs of apoptosis as well as caspase-3 and Bax proteins, but strongly positive for bcl-2.

It is of interest that clinorotation triggered endothelial cells to enhance the production of VEGF and of VEGF receptor by themselves (Figure 4). VEGFs comprise a family of secreted polypeptides with a highly conserved receptor-binding cystine-knot structure.[30] The different family members VEGF, VEGF-beta, placental growth factor (PIGF), VEGF-C and VEGF-D bind specifically to their respective receptors VEGFR-1, -2 and -3, which differ considerably in signaling properties.[32,66] VEGFR-2/KDR/Flk-1 found in this study to be enhanced during clinorotation is a high-affinity receptor for VEGF-A, and mediates most of the endothelial growth and survival signals from VEGF-A.[67] Still the autocrine loop turned on during clinorotation appears to be too weak to counterbalance effectively the influence of an environment lacking a gravity vector.

Alterations of the cytoskeleton

Eukaryotic cells are very sensitive to changes in gravity, because the location of cellular components depends on the integrity and spatial organization of the cytoskeletal architecture (microtubules, microfilaments and intermediate filaments) and the nucleoskeleton. The organization of these cellular compartments and signal proteins is regulated by extracellular signals, cell-cell and cell-extracellular matrix (ECM) signaling.[68,69] Moreover, the cytoskeleton is affected by weightlessness in several types of cells such as thyrocytes,[11] osteoblasts,[55] lymphocytes,[15] glial cells,[13] and breast cancer cells.[12] We also could demonstrate alterations of microtubules and intermediate filaments which were thicker and increased after 24 h of culture under conditions of simulated microgravity. These cellular alterations appear to be responsible for observations made on astronauts and experimental animals during and after a stay in orbit. These health problems in astronauts are amongst others impaired bone healing, muscle atrophy and cardiovascular problems including alterations of the vascular endothelium.[1]

Conclusions

We have shown that clinorotation of endothelial cells is an interesting new method in investigating the formation of tube-like three-dimensional endothelial cell aggregates, and may be useful to learn more about the cascade of biochemical reactions initiated by binding of VEGF to its receptor.[70] Flk-1 was induced in endothelial cells cultured under simulated microgravity. In this context, a three-dimensional clinostat provides a convenient experimental system to culture many endothelial cells grown in the form of tubes, consisting of cells progressing through apoptosis and others resistant to apoptosis. Therefore, clinorotation represents an important ground based facility model system for studying the effects of reduced gravity on cells.

Our results provide new information on human endothelial cells grown under simulated microgravity. Apoptosis is initiated within 4 h. In parallel, the expression of extracellular matrix proteins and promoters and inhibitors of apoptosis increased. Programmed cell death is induced via extrinsic and intrinsic pathways. This information may help to find the roots of the negative physiological changes which humans and animals face during a longer stay in the orbit.[1]

Acknowledgment

Our research was supported by the German Space Agency DLR (grant 50WB0524). We thank the Space Biology group, ETH Zurich Switzerland, for providing the clinostat and lab facilities. We thank Dr. Chris Talsness and Jessie Webb (BSc) for editing English language.

References

1. White RJ, Averner M. Humans in space. *Nature* 2001; **409**: 1115–1118.
2. Baldwin KM. Effect of spaceflight on the functional, biochemical, and metabolic properties of skeletal muscle. *Med Sci Sports Exerc* 1996; **28**: 983–987.
3. Fritsch-Yelle JM, Leuenberger UA, D'Aunno DS, *et al*. An episode of ventricular tachycardia during long-duration spaceflight. *Am J Cardiol* 1998; **81**: 1391–1392.
4. Levine BD, Zuckerman JH, Pawelczyk JA. Cardiac atrophy after bed-rest deconditioning: a non-neural mechanism for orthostatic intolerance. *Circulation* 1997; **96**: 517–525.
5. Young LR, Oman CM, Watt DGD, Money KE, Lichtenberg BK. Spatial orientation in weightlessness and readaptation to Earth's gravity. *Science* 1984; **225**: 205–208.
6. Buckey JC Jr, Lane LD, Levine BD, *et al*. Orthostatic intolerance following spaceflight. *J Appl Physiol* 1996; **81**: 7–18.
7. Reyes C, Freeman-Perez S, Fritsch-Yelle JM. Orthostatic intolerance following short and long duration flight. *FASEB J* 1999; **13**: A1048.
8. Gündel A, Polyakov VV, Zulley J. The alteration of human sleep and circadian rhythms during spaceflight. *J Sleep Res* 1997; **6**: 1–8.

9. Taylor GR. Overview of spaceflight immunology studies. *J Leukoc Biol* 1993; **54**: 179–188.
10. Gmünder FK, Cogoli A. In: (Fregly, M. J. & Blatteis, C. M. eds;) *Handbook of Physiology. Section 4: Environmental Physiology* American Physiological Society, New York: 1996: 799–814.
11. Grimm D, Bauer J, Kossmehl P, *et al*. Simulated microgravity alters differentiation and increases apoptosis in human follicular thyroid carcinoma cells. *FASEB J* 2002; **16**: U55–U81.
12. Vassy J, Portet S, Beil M, *et al*. The effect of weightlessness on cytoskeleton architecture and proliferation of human breast cancer cell line MCF-7. *FASEB J* 2001; **15**: 1104–1106.
13. Uva BM, Masini MA, Sturla M, *et al*. Clinorotation-induced weightlessness influences the cytoskeleton of glial cells in culture. *Brain Res* 2002; **934**: 132–139.
14. Boonyaratanakornkit JB, Cogoli A, Li CF, *et al*. Key gravity-sensitive signaling pathways drive T-cell activation. *FASEB J* 2005 Oct 6; [Epub ahead of print]
15. Lewis ML, Cubano LA, Zhao B, *et al*. cDNA microarray reveals altered cytoskeletal gene expression in space-flown leukemic T lymphocytes (Jurkat). *FASEB J* 2001; **15**: 1783–1785.
16. Hammond TG, Benes E, O'Reilly KC, *et al*. Mechanical culture conditions effect gene expression: gravity induced changes on the space shuttle. *Physiol Genomics* 2000; **3**: 163–173.
17. Kossmehl P, Shakibaei M, Cogoli A, *et al*. Weightlessness induced apoptosis in normal thyroid cells and papillary thyroid carcinoma cells via extrinsic and intrinsic pathways. *Endocrinology* 2003; **144**: 4172–4179.
18. Pardo SJ, Patel MJ, Sykes MC, *et al*. Simulated microgravity using the Random Positioning Machine inhibits differentiation and alters gene expression profiles of 2T3 preosteoblasts. *Am J Physiol-Cell Physiol* 2005; **288**: C1211–C1221.
19. Clejan S, O'Connor K, Rosensweig N. Tri-dimensional prostate cell cultures in simulated microgravity and induced changes in lipid second messengers and signal transduction. *J Cell Mol Med* 2001; **5**: 60–73.
20. Martin A, Zhou A, Gordon RE, *et al*. Thyroid organoid formation in simulated microgravity: Influence of keratinocyte growth factor. *Thyroid* 2000; **10**: 481–487.
21. Chopra V, Dinh TV, Hannigan EV. Three-dimensional endothelial-tumor epithelial cell interactions in human cervical cancers. *In Vitro Cell Dev Biol Animal* 1997; **33**: 432–442.
22. Buravkova L, Romanov Y, Rykova M, Grigorieva O, Merzlikina N. Cell-to-cell interactions in changed gravity: Ground-based and flight experiments. *Acta Astronatutica* 2005; **57**: 67–74.
23. Sangha DS, Han S, Purdy RE.Simulated microgravity upregulates an endothelial vasoconstrictor prostaglandin.*J Applied Physiol* 2001; **91**: 789–796.
24. Schiffrin EL. The endothelium and control of blood-vessel function in health and disease. *Clin Invest Med* 1994; **17**: 602–620.
25. Aird WC. Spatial and temporal dynamics of the endothelium. *J Thromb Haemost* 2005; **3**: 1392–1406.
26. Li K, Sirois P, Rouleau JL. Role of endothelial-cells in cardiovascular function. *Life Sci* 1994; **54**: 579–592.
27. Michiels C. Endothelial cell functions. *J Cell Physiol* 2003; **196**: 430–443.
28. Tang DG, Conti CJ. Endothelial cell development, vasculogenesis, angiogenesis, and tumor neovascularization: An update. *Semin Thromb Hemost* 2004; **30**: 109–117.
29. Scrofani SDB, Nash AD. Towards a structure-function relationship for vascular endothelial growth factor-B (VEGF-B). *J Microbiol Biotechnol* 2001; **11**: 543–551.
30. Holmes DI, Zachary I. The vascular endothelial growth factor (VEGF) family: angiogenic factors in health and disease. *Genome Biol* 2005; **6**: 209.
31. Brockington A, Lewis C, Wharton S, Shaw PJ. Vascular endothelial growth factor and the nervous system. *Neuropathol & Applied Neurobio* 2004; **30**: 427–446.
32. Tammela T, Enholm B, Alitalo K, Paavonen K. The biology of vascular endothelial growth factors. *Cardiovasc Res* 2005; **65**: 550–563.
33. Zachary I. Signaling mechanisms mediating vascular protective actions of vascular endothelial growth factor. *Am J Physiol Cell Physiol* 2001; **280**: C1375–C1386.
34. Hoson T, Kamisaka S, Masuda Y, Yamashita M. Changes in plant growth processes under microgravity conditions simulated by a three-dimensional clinostat. *Bot Mag* 1992; **105**: 53–70.
35. Emeis JJ, Edgell CJS. Fibrinolytic properties of a human endothelial hybrid cell-line (EA.hy926). *Blood* 1988; **71**: 1669–1675.
36. Grimm D, Huber M, Jabusch HC, *et al*. Extracellular matrix proteins in cardiac fibroblasts derived from rat hearts with chronic pressure overload: effects of beta-receptor blockade. *J Mol Cell Cardiol* 2001; **33**: 487–501.
37. Grimm D, Kromer EP, Böcker W, *et al*. Regulation of extracellular matrix proteins in pressure-overload cardiac hypertrophy: effects of angiotensin-converting enzyme inhibition. *J Hypertens* 1998; **16**: 1345–1355.
38. Grimm D, Bauer J, Hofstädter F, Riegger GAJ, Kromer EP. Characteristics of multicellular spheroids formed by primary cultures of human thyroid tumor cells. *Thyroid* 1997; **7**: 859–865.
39. Shakibaei M, Zimmermann B, Merker HJ. Changes in integrin expression during chondrogenesis in vitro: an immunomorphological study. *J Histochem Cytochem* 1995; **43**: 1061–1069
40. Kossmehl P, Schonberger J, Shakibaei M, *et al*. Increase of fibronectin and osteopontin in porcine hearts following ischemia and reperfusion. *J Mol Med* 2005; **83**: 626–637.
41. Margolis L, Hatfill S, Chuaqui R, *et al*. Long term organ culture of human prostate tissue in a NASA-designed rotating wall bioreactor. *J Urol* 1999; **161**: 290–297.
42. Khaoustov VI, Darlington GJ, Soriano HE, *et al*. Induction of three-dimensional assembly of human liver cells by simulated microgravity. *In Vitro Cell Dev Biol Anim* 1999; **35**: 501–509.
43. Zhau HE, Goodwin TJ, Chang SM, Baker TL, Chung LW. Establishment of a three-dimensional human prostate organoid coculture under microgravity-simulated conditions: evaluation of androgen-induced growth and PSA expression. *In Vitro Cell Dev Biol Anim* 1997; **33**: 375–380.
44. Sakar D, Nagaya T, Koga K, Nomura Y, Gruener R, Seo H. Culture in vector-averaged gravity under clinostat rotation results in apoptosis of osteoblastic ROS 17/2.8 cells. *J Bone Miner Res* 2000; **15**: 489–498.
45. Ingram M, Techy GB, Saroufeem R, *et al*. Three-dimensional growth patterns of various human tumor cell lines in simulated microgravity of a NASA bioreactor. *In Vitro Cell Dev Biol Anim* 1997; **33**: 459–466.
46. Cogoli M. The fast rotating clinostat: a history of its use in gravitational biology and a comparison of ground-based and flight experiment results. *ASGSB Bull* 1992; **5**: 59–67.
47. Hammond TG, Hammond JM. Optimized suspension culture: the rotating-wall vessel. *Am J Physiol Renal Physiol* 2001; **281**: F12–25.
48. Schwarzenberg M, Pippia P, Meloni MA, Cossu G, Cogoli-Greuter M, Cogoli A. Microgravity simulations with human lymphocytes in the free fall machine and in the random positioning machine. *J Grav Physiol* 1998; **5**: P23–P26.
49. Bauer J, Margolis M, Schreiner C, *et al*. *In vitro* model of angiogenesis using a human endothelium-derived permanenet cell-line — Contributions of induced gene expression, G-proteins, and integrins. *J Cell Physiol* 1992; **153**: 437–449.
50. Shiose S, Hata Y, Noda Y, *et al*. Fibrinogen stimulates in vitro angiogenesis by choroidal endothelial cells via autocrine VEGF. *Graefes Arch Clin Exp Ophtalmol* 2004; **242**: 777–783.
51. Kim HK, Song KS, Chung JH, Lee KR, Lee SN. Platelet microparticles induce angiogenesis in vitro. *British J Haematol* 2004; **124**: 376–384.

52. McCloskey KE, Gilroy ME, Nerem RM. Use of embryonic stem cell-derived endothelial cells as a cell source to generate vessel structures *in vitro*. *Tissue Eng* 2005; **11**: 497–505.
53. Oishi K, Kobayashi A, Fujii K, Kanehira D, Ito Y, Uchida MK. Angiogenesis in vitro: Vascular tube formation from the differentiation of neural stem cells. *J Pharmacol Sci* 2004; **96**: 208–218.
54. Hsu SH, Kuo CC, Yen HJ, Whu SW, Tsai CL. The effect of two different bioreactors on the neocartilage formation in type II collagen modified polyester scaffolds seeded with chondrocytes. *Artifical Organs* 2005; **29**: 467–474.
55. Hughes-Fulford M. Function of the cytoskeleton in gravisensing during spaceflight. *Adv Space Res* 2003; **32**: 1585–1593.
56. Davis GE, Bayless KJ, Mavila A. Molecular Basis of Endothelial Cell Morphogenesis in Three-Dimensional Extracellular Matrices. *Anat Record* 2002; **268**: 252–275.
57. Albig AR, Schiemann WP. Fibulin-5 antagonizes vascular endothelial growth factor (VEGF) signaling and angiogenic sprouting by endothelial cells. *DNA Cell Biol* 2004; **23**: 367–379.
58. Solovey A, Gui LZ, Ramakrishnan S, Steinberg MH, Hebbel RP. Sickle cell anemia as a possible state of enhanced anti-apoptotic tone: Survival effect of vascular endothelial growth factor on circulating and unanchored endothelial cells. *Blood* 1999; **93**: 3824– 3830.
59. Avraham HK, Lee TH, Koh YH, *et al*. Vascular endothelial growth factor regulates focal adhesion assembly in human brain microvascular endothelial cells through activation of the focal adhesion kinase and related adhesion focal tyrosine kinase. *J Biol Chem* 2003; **278**: 36661–36668.
60. Adams JM, Cory S. Life-or-death decisions by the Bcl-2 protein family. *Trends Biochem Sci* 2001; **26**: 61–66.
61. Lewis ML, Reynolds JL, Cubano LA, Hatton JP, Lawless BD, Piepmeier EH. Spaceflight alters microtubules and increases apoptosis in human lymphocytes (Jurkat). *FASEB J* 1998; **12**: 1007–1018.
62. Maccarrone M, Battista N, Meloni M, *et al*. Creating conditions similar to those that occur during exposure of cells to microgravity induces apoptosis in human lymphocytes by 5-lipoxygenase-mediated mitochondrial uncoupling and cytochrome c release. *J Leukoc Biol* 2003; **73**: 472–481.
63. Watanabe Y, Dvorak HF. Vascular permeability factor vascular endothelial growth factor inhibits anchorage-disruption-induced apoptosis in microvessel endothelial cells by inducing scaffold formation. *Exp Cell Res* 1997; **233**: 340–349.
64. Spyridopoulos I, Brogi E, Kearney M, *et al*. Vascular endothelial growth factor inhibits endothelial cell apoptosis induced by tumor necrosis factor-alpha: Balance between growth and death signals. *J Mol Cell Cardiol* 1997; **29**: 1321–1330.
65. Morbidelli L, Monici M, Marziliano N, *et al*. Simulated hypogravity impairs the angiogenic response of endothelium by up-regulating apoptotic signals. *Biochem Biophys Res Commun* 2005; **334**: 491–499.
66. Ferrara N, Gerber HP, LeCouter J. The biology of VEGF and its receptors. *Nature Medicine* 2003; **9**: 669–676.
67. Shibuya M. Vascular endothelial growth factor receptor-2: Its unique signaling and specific ligand, VEGF-E. *Cancer Science* 2003; **94**: 751–756.
68. Lelievre SA, Weaver VM, Nickerson JA, *et al*. Tissue phenotype depends on reciprocal interactions between the extracellular matrix and the structural organization of the nucleus. *Proc Natl Acad Sci USA* 1998; **95**: 14711–14716.
69. Roskelley CD, Desprez PY, Bissell MJ. Extracellular matrix-dependent tissue-specific gene expression in mammary epithelial cells requires both physical and biochemical signal transduction. *Proc Natl Acad Sci USA* 1994; **91**: 12378–1238.
70. Hippenstiel S, Krull M, Ikemann A, Risau W, Clauss M, Suttorp N. VEGF induces hyperpermeability by a direct action on endothelial cells. *Am J Physiol Lung Cell Mol Physiol* 1998; **18**: L678–L684.